

The weakening of the ENSO–Indian Ocean Dipole (IOD) coupling strength in recent decades

Yoo-Geun Ham¹ · Jun-Young Choi¹ · Jong-Seong Kug²

Received: 14 March 2016 / Accepted: 30 August 2016 / Published online: 12 September 2016
© Springer-Verlag Berlin Heidelberg 2016

Abstract This study examines a recent weakening of the coupling between the El Niño–Southern Oscillation (ENSO) and the Indian Ocean Dipole (IOD) mode after the 2000s and 2010s compared to the previous two decades (1980s and 1990s). The correlation between the IOD during the September–November season and the Niño3.4 index during the December–February season is 0.21 for 1999–2014, while for the previous two decades (1979–1998) it is 0.64. It is found that this weakening of the ENSO–IOD coupling during the 2000s and 2010s is associated with different spatial patterns in ENSO evolution during the boreal spring and summer seasons. During the boreal spring season of the El Niño developing phase, positive precipitation anomalies over the northern off-equatorial western Pacific is systematically weakened during the 2000s and 2010s. This also weakens the low-level cross-equatorial southerly flow, which can cause local negative precipitation anomalies over the maritime continent through increased evaporation and cold and dry moist energy advection. The weakened negative precipitation anomalies over the maritime continent reduces the amplitude of the equatorial easterly over the IO, therefore, suppresses a ENSO-related IOD variability. An analysis using climate models that participated in the Coupled Model Intercomparison Project phase 5 (CMIP5) supports this observational findings that the amplitude of the cross-equatorial southerly flow and associated suppressed convective activities over the maritime

continent during the El Niño developing season are critical for determining the ENSO–IOD coupling strength in climate models.

Keywords ENSO · Indian Ocean Dipole · Decadal modulation

1 Introduction

The coupling between the El Niño–Southern Oscillation (ENSO) and the Indian Ocean Dipole (IOD) mode is of considerable interest (Webster et al. 1999; Allan et al. 2001) as this can significantly modulate the global teleconnection pattern during ENSO events (Ashok et al. 2001; Behera and Yamagata 2003; Cai et al. 2011; Weller and Cai 2013). In addition, once the IOD is co-occurred with the ENSO, it also acts to fasten the phase transition of the ENSO (Kug and Kang 2006; Kug et al. 2006a, b; Luo et al. 2010; Izumo et al. 2010; Kug and Ham 2012). This implies that the coupling between the ENSO and the IOD can influence not only the global teleconnection pattern, but also the ENSO evolution itself.

However, the detailed coupling process between the ENSO and the IOD is still not clear which leads the diverse previous literatures about the ENSO and the IOD coupling. As part of the discussion about whether IOD is not relevant to the ENSO (Saji et al. 1999; Allan et al. 2001; Behera et al. 2006), modeling experiments showed contrasting results with regard to the independency of the IOD from the ENSO (Behera et al. 2000; Iizuka et al. 2000; Baquero-Bernal et al. 2002). Allan et al. (2001) suggested that there is some ENSO-related IOD variability, but that some IOD events may be induced by an ENSO-independent processes over the Indian Ocean (IO). Hong et al. (2008) supported

✉ Jong-Seong Kug
jskug@postech.ac.kr

¹ Department of Oceanography, Chonnam National University, Gwangju, South Korea

² School of Environmental Science and Engineering, Pohang University of Science and Technology, Pohang, South Korea

this argument that IOD events can be categorized as the IOD with and without the influence of ENSO, and that there is systematic difference in the temporal evolution and the spatial distribution between those events. This was also shown in long-term numerical simulations (Lau and Nath 2004), which implied that some IOD events could be induced by intrinsic air–sea coupled feedbacks over the IO, while some were excited by ENSO.

Assuming that the IOD can be decomposed into ENSO-independent and ENSO-dependent components, a relative amplitude change of those components at decadal time scales can result in a decadal modulation of the ENSO–IOD relationship (Ashok et al. 2001, 2004; Ashok and Saji 2007; Yuan and Li 2008; Ummenhofer et al. 2011; Izumo et al. 2014). Yuan and Li (2008) showed that ENSO and IOD were independent from each other during 1948–1969, while ENSO–IOD coupling became strong after 1970. Ashok et al. (2001) argued the coupling between ENSO and the Indian summer monsoon rainfall (ISMR) could be weakened when IOD–ISMR coupling is strong. This is further supported by the authors' subsequent works using climate model (Ashok et al. 2004; Ashok and Saji 2007). Similarly, Ummenhofer et al. (2011) found that during El Niño events coupled with positive IOD events, ISMR anomalies are relatively weaker than during El Niño-only events, because positive IOD events tend to increase ISMR anomalies, while ENSO tends to reduce those anomalies. This implies that deciphering the mechanism that controls the ENSO–IOD relationship is key to understanding the ENSO–ISMR relationship.

The IOD event is strongly coupled to the surface wind variability over the central IO (Saji et al. 1999), which might denote that the oceanic feedback induced by the surface wind forcing is crucial to the generation of the IOD like the El Niño Southern Oscillation (ENSO) (Li et al. 2003). However, the systematic different oceanic states in the Indian Ocean from those in the Pacific prevent the ENSO-like variability over the Indian Ocean. That is, the deep mean thermocline over the eastern IO prevents an oceanic Rossby wave and the associated subsurface temperature variability from linking to the SST variability (Li et al. 2003). While the surface heat flux is mainly a damping mechanism for the ENSO, the latent heat flux and the vertical temperature advection is important to induce the IOD event over the eastern IO (Li et al. 2002). In addition, it is found that the former leads the surface cooling during the IOD by a few months, while the latter is in phase with the SSTA, which implies that the latent heat flux is critical to generate the IOD over the eastern IO. This is further supported by later studies using long-term climate models (Hong et al. 2008). In addition, Li et al. (2003) mentioned that IOD develops during the boreal summer season when the climatological southeasterly is dominant over

the south-eastern IO, which infers wind–evaporation–SST (WES) feedback induced by the anomalous southeasterly is crucial to induce the surface cooling over the eastern IO. On the other hand, with aids of the shallow thermocline, the IOD over the western IO is mainly generated by the oceanic process such as meridional and vertical temperature advection (Webster et al. 1999; Ueda and Matsumoto 2000; Li et al. 2003).

However, although previous researches about the ENSO–IOD coupling, it is still not clear what causes the decadal modulation of the strength of the ENSO–IOD coupling. In addition, the decadal modulation during the recent decade has not yet been investigated as most of the studies on the decadal modulation of the relationship between ENSO and the Indian Ocean variability have used data covering the period up to the early 2000s (i.e., mostly until 2006, as in the case of the Indian Institute of Tropical Meteorology (IITM)). A possible change in the ENSO–IOD relationship during the recent decade is especially important because of the occurrence of the central Pacific El Niño (Yeh et al. 2009), or the recent La Niña-like background change possibly induced by the Indian Ocean warming (Luo et al. 2012). Therefore, it is essential to examine any systematic differences in the ENSO–IOD relationship between the recent and previous decades.

Therefore, this study investigates the decadal modulation of the ENSO–IOD relationship during the recent decade (2000s and 2010s) using reanalysis data. In addition, the findings will be evaluated by climate model simulations in the Coupled Model Intercomparison Project phase 5 (CMIP5). In Sect. 2, observational data and the model output used in this study are summarized. Section 3 provides the observational evidence for a weakening of the ENSO–IOD coupling during the 2000s and 2010s compared to the previous two decades (1980s and 1990s). In Sect. 4, the CMIP5 model results, which support the observational findings, will be shown. A summary and discussion are provided in Sect. 5.

2 Data

The sea surface temperature (SST) data were derived from the Extended Reconstructed Sea Surface Temperature version 3b (ERSST V.3b; Smith and Reynolds 2004), HadISST v1.1 (Rayner et al. 2003), and Optimum Interpolation SST (OISST) v.2 (Reynolds et al. 2002) from NOAA. The monthly data of three-dimensional moisture, temperature, wind, and surface heat flux are from the ERA-INTERIM (Dee et al. 2011). The precipitation data collected by the Global Precipitation Climatology Project (GPCP) were used for 1979 to 2014 (Adler et al. 2003). For the model

Table 1 List of model from the CMIP5 archives

Model number	Model name	Integration period (years)
1	CNRM-CM5	156
2	CESM1-CAM5	156
3	GFDL-ESM2M	156
4	GFDL-CM3	156
5	NorESM1-ME	156
6	bcc-csm1-1-m	156
7	NorESM1-M	156
8	MPI-ESM-LR	156
9	CMCC-CMS	156
10	MIROC5	156
11	BNU-ESM	156
12	FIO-ESM	156
13	CESM1-BGC	156
14	GFDL-ESM2G	156
15	GISS-E2-R	156
16	CCSM4	156
17	IPSL-CM5A-MR	156
18	IPSL-CM5B-LR	156
19	CMCC-CM	156
20	bcc-csm1-1	156
21	IPSL-CM5A-LR	156
22	MRI-CGCM3	156
23	GISS-E2-H-CC	156
24	HadGEM2-ES	146
25	HadGEM2-CC	146
26	GISS-E2-H	156
27	GISS-E2-R-CC	156
28	MPI-ESM-MR	156
29	HadGEM2-AO	156
30	CanESM2	156
31	inmcm4	156
32	CSIRO-Mk3-6-0	156
33	MIROC-ESM	156
34	MIROC-ESM-CHEM	156

output, we analyzed 34 climate models from historical simulation of CMIP5 (Ham and Kug 2015). Table 1 provides a list of those models. All data were de-trended before analysis.

3 Mechanisms for the observed weakening of the ENSO–IOD coupling after 2000

To illustrate the decadal variation of the strength of the ENSO–IOD coupling, Fig. 1 shows the 15-year moving correlation between the Nino3.4 index (SSTA over 170°W–120°W, 5°S–5°N) during the DJF season and

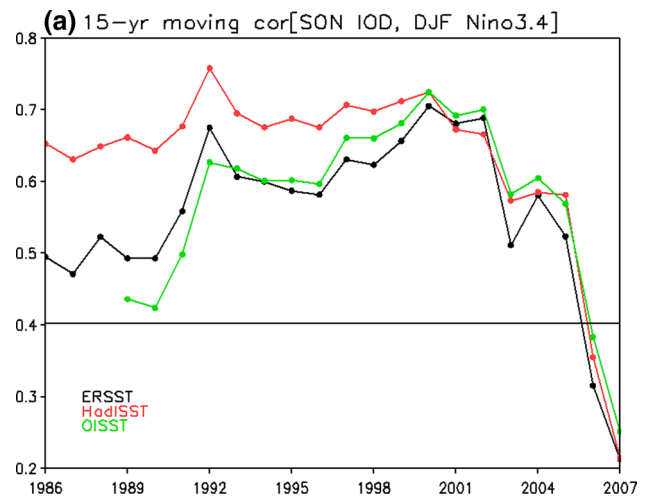


Fig. 1 Fifteen-year moving correlation between the Nino3.4 index (SSTA averaged over 170°–120°W, 5°S–5°N) during the December–February (DJF) season and the IOD index (SSTA differences over the western IO (50°–70°E, 10°S–10°N) to the eastern IO (90°–110°E, 10°–0°S) during the September–November (SON) season using three different SST products (*black*: ERSST v.3b, *red*: HadISST v1.1, *green*: OISST v.2)

the IOD index (SSTA differences over the western IO (50°E–70°E, 10°S–10°N) to the eastern IO (90°E–110°E, 10°S–0°)) during the SON season. Note that the choice of season for the ENSO or the IOD index is based on the peak season of the ENSO and the IOD event, which is often used to examine the ENSO–IOD relationship (Yuan and Li 2008; Hong et al. 2008, 2010). Three different SST products (i.e., ERSST v.3b, Hadisst v1.1, and OISST v.2) consistently show that the correlation during 1980s and 1990s is above 0.5, significant over the 95 % confidence level, indicating a strong coupling between the ENSO and the IOD. This supports arguments in previous literatures that the weakening of the inverse ENSO–ISMR relationship during the 1980s and 1990s was associated with a strengthening of the ENSO–IOD coupling (Ashok et al. 2001). However, all SST products also clearly exhibit that this strong coupling between ENSO and IOD systematically weakened during the 2000s and 2010s. For example, the correlation between ENSO and IOD from ERSST v.3b for 1999–2013 is only about 0.3 and only 0.21 for 2000–2014. This feature is still clear when the Nino3.4 index during boreal summer or fall season is used (not shown).

To examine the change in the ENSO–IOD relationship in more detail, Fig. 2 shows the time-series of the DJF Nino3.4 and SON IOD from 1979 to 2014. During 1979–1998, among six cases whose Nino3.4 index is over 0.5 standard deviation (std), IOD index is over 1 std for five cases. On the other hand, during 1999–2014, among five cases that Nino3.4 is greater than 0.5 std, only two case exhibits IOD index greater than 0.5 standard deviation. In

Fig. 2 Normalized time series of the D(0)JF(1) Nino3.4 (black bar), and SON(0) IOD index (red line) from 1979 to 2014

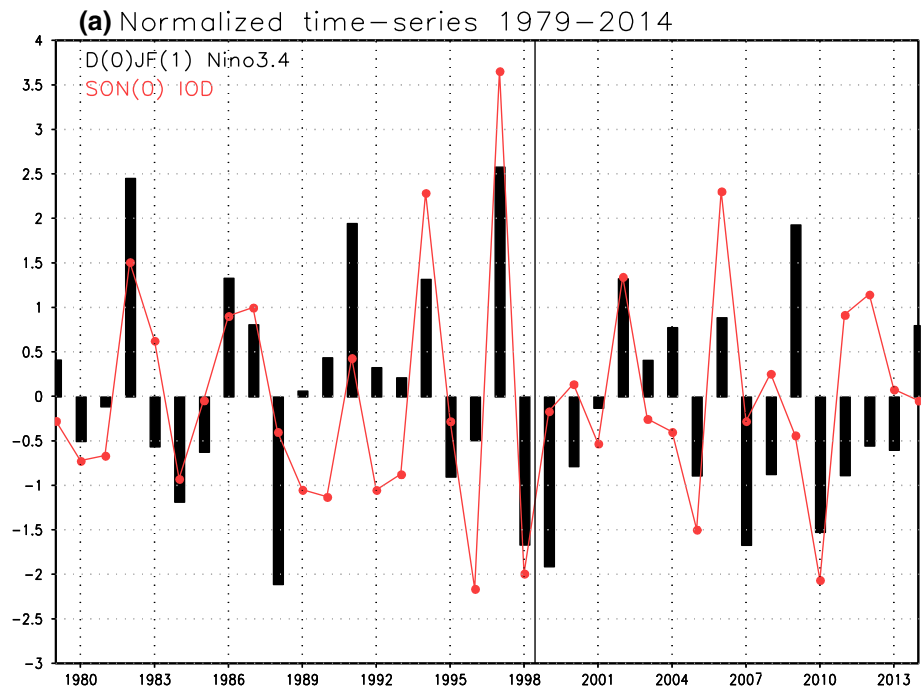
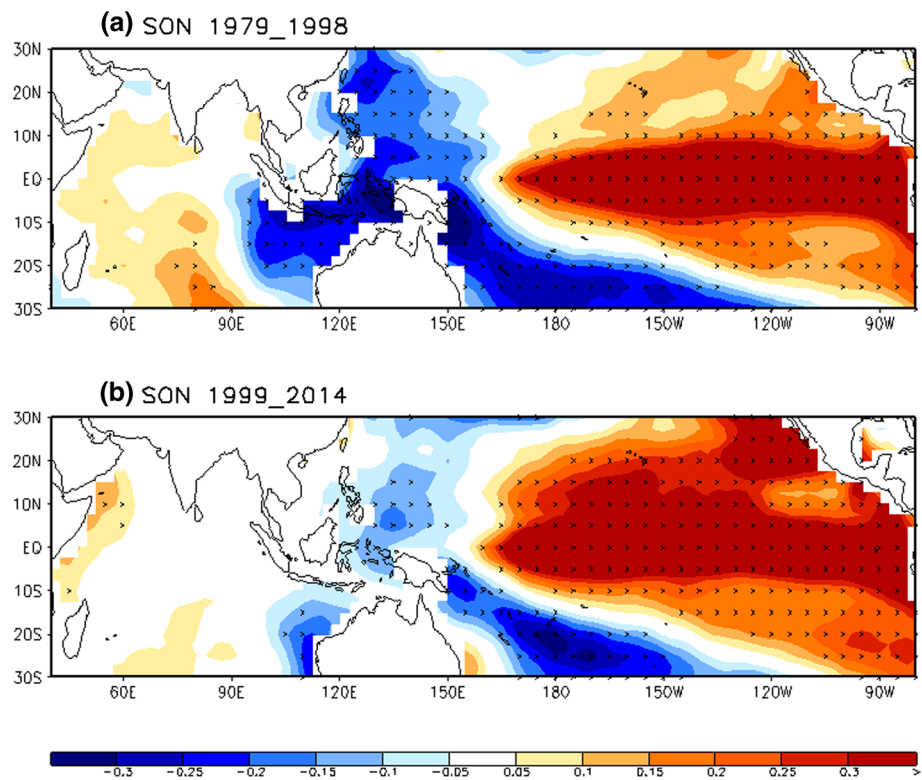


Fig. 3 Lag-regression of normalized ERSST v.3b SST anomalies during the SON season against the Nino3.4 index during the DJF season for **a** 1979–1998 and **b** 1999–2014. The values over 95 % confidence level based on the student *t* test are denoted by black dots



addition, the relationship between the La Nina and negative IOD is systematically weakened during 1999–2014. For example, the four of seven La Nina events, which is defined as DJF Nino3.4 index is smaller than -0.5 std, are with negative IOD events during 1979–1998 periods, while only two of seven La Nina events are with negative IOD

events. This clearly indicates that the ENSO-IOD coupling is weakened during 1999–2014.

The spatial distribution of ENSO-related SST anomalies during the SON season also exhibits consistent results. Figure 3 is the lag-regression of SST anomalies during the SON season onto the DJF Nino3.4 index. The

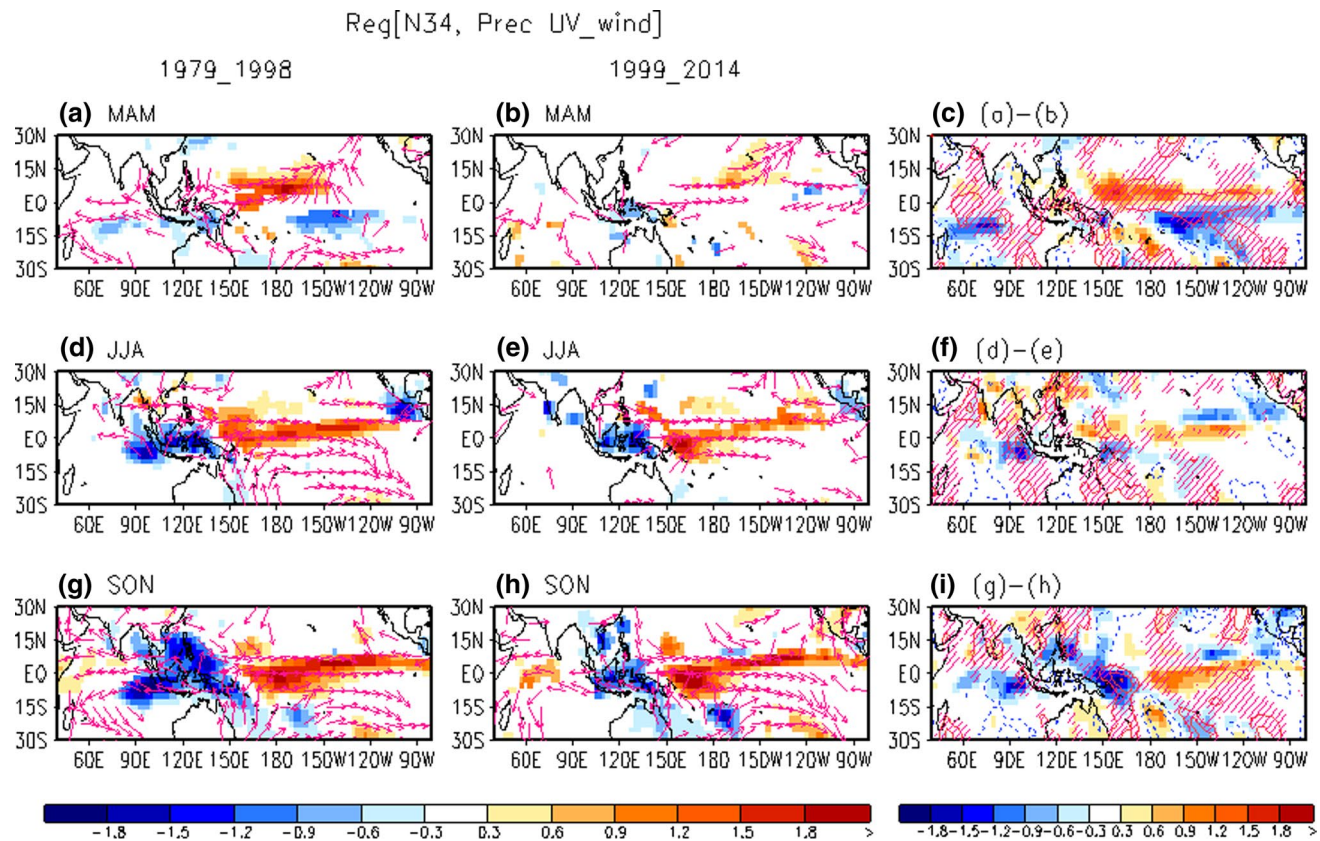


Fig. 4 Nino3.4-regressed precipitation (*shading*) and 850-hPa wind vector anomalies during the MAM (*upper panel*), JJA (*middle panel*), and SON (*lower panel*) seasons of 1979–1998 (*left*), and 1999–2014 (*middle*). The difference in the regression of precipitation (*shading*) and 850-hPa meridional wind (*contour*) anomalies between the two

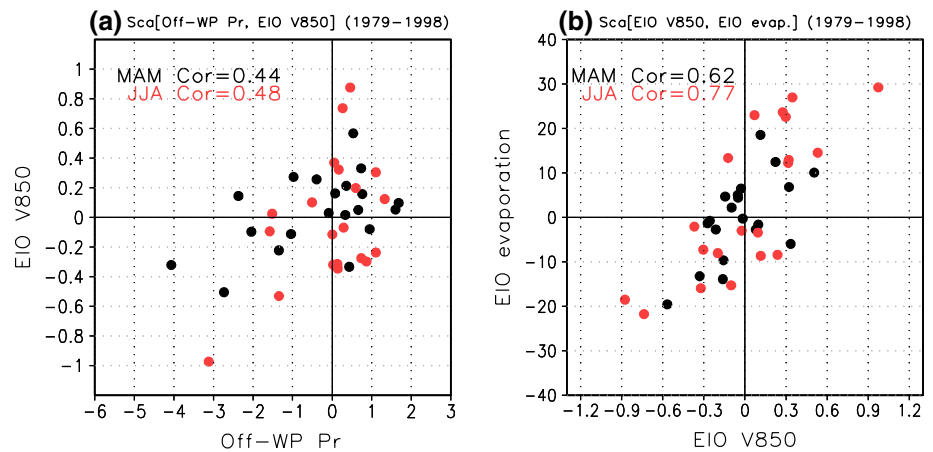
decades is shown in the *panels on the right*. The *red oblique line* in the panels on the *right* denotes the area where the difference of the 850-hPa meridional wind is positive. Only the values over 95 % confidence level based on the student *t* test are drawn

ENSO-related SST anomalies during 1979–1998 show distinctive negative anomalies over the eastern IO and the western Pacific, while positive SST anomalies are shown over the western IO, although the latter are relatively weak. On the other hand, SST signals over the IO are hardly seen during 1999–2014 (Fig. 3b). This implies that the coupling between the ENSO and the IOD significantly weakened during the 2000s and 2010s, which is consistent with Fig. 1. This weakening of the ENSO–IOD relationship may have resulted in a decreased IOD amplitude during SON in recent decades. The standard deviation of the IOD index decreased from 0.41 for 1979–1998 to 0.31 for 1999–2014.

This significant weakening in the ENSO–IOD coupling during the 2000s and 2010s can be explained by differences in ENSO evolution. Figure 4 shows the Nino3.4-regressed precipitation and circulation anomalies during the El Niño developing seasons during 1979–1998 and during 1999–2014. At the El Niño-developing MAM season of 1979–1998, precipitation anomalies exhibit positive values over the northern off-equatorial western-central Pacific. This induces low-level westerly anomalies over the

western-central Pacific, which contributes to the development of the El Niño (Jin 1997; Kug et al. 2010). The weakening of the upward branch of zonal Walker Circulation over the maritime continent might be related to the equatorial easterly over the IO during 1979–1998, which can help to induce the positive IOD event. In addition, these positive off-equatorial precipitation anomalies denote a hemispheric asymmetry of atmospheric heating, which can induce a cross-equatorial southerly flow based on the Gill-type response (Gill 1980). However, the cross-equatorial southerly is not clear during the El Niño-developing MAM seasons of 1999–2014, possibly due to the weakened off-equatorial precipitation anomalies over the western Pacific. The difference map in Fig. 4c clearly shows stronger positive anomalous precipitation over the off-equatorial western Pacific with a stronger anomalous southerly over the maritime continent during the previous decades. Note that this feature is still clear when the same season for the Nino3.4 index to that for the IOD index (i.e. SON) is used (not shown). During the June–August (JJA) seasons of 1979–1998, the cross-equatorial southerly flow and the negative

Fig. 5 **a** Scatter diagram for ENSO-related precipitation anomalies in the off-equatorial western Pacific (120° – 160° E, 0° – 15° N) and 850-hPa meridional wind over the eastern IO (90° – 110° E, 10° – 0° S) for 1979–1998; **b** scatter diagram for 850-hPa meridional wind and evaporation over the eastern IO (90° – 110° E, 10° – 0° S)



anomalous precipitation extend to the eastern IO (Fig. 4d), while the anomaly is confined to the western Pacific during 1999–2014 (Fig. 4e). The negative anomalous precipitation in the eastern IO is a key to trigger the positive IOD event through the Bjerknes feedback during subsequent season. That is, the negative precipitation anomalies over the eastern IO during JJA generates the equatorial easterly over the central IO, it induces the positive SST anomalies over the western IO by exciting oceanic Rossby waves (Saji et al. 1999; Li et al. 2003). With aids of this Bjerknes feedback, the positive IOD event is induced during SON season with enhanced equatorial easterly over the IO in 1979–1998, while it is systematically weaker during 1999–2014.

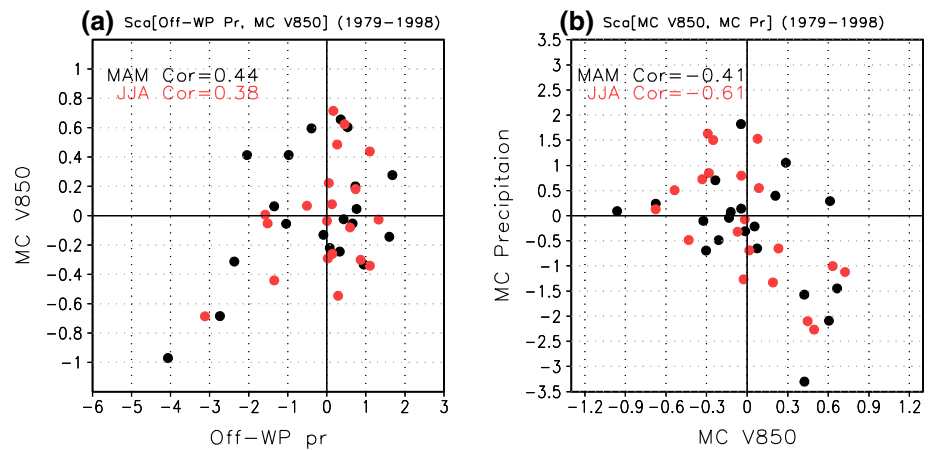
Li et al. (2002) and Sooraj et al. (2009) pointed out that the cross-equatorial southerly over the eastern IO increases total wind speed, leading to a cold sea surface. These negative anomalous SST over the eastern IO help to develop the positive IOD event by inducing suppressed motions with the equatorial easterly over the central IO. Figure 5a shows a scatter diagram for precipitation over the western Pacific (120° E to 160° E, 0° to 15° N) and 850-hPa meridional wind over the eastern IO (90° E– 110° E, 10° S– 0°) for 1979–1998, which supports Li et al.'s (2002) and Sooraj et al.'s (2009) findings. The increased precipitation over the off-equatorial western Pacific is correlated with the southerly flow over the eastern IO for both the MAM and JJA seasons. Correlation coefficients are 0.44 for the MAM season and 0.48 for the JJA season. This indicates that the anomalous precipitation over the off-equatorial western Pacific can induce the southerly flow over the eastern IO. Once this southerly flow is induced over the eastern IO, it increases the local evaporation that is associated with the cold SST anomalies. Figure 5b shows a scatter diagram for the 850-hPa meridional wind and the evaporation over the eastern IO. The correlation are 0.62 for the MAM season and 0.77 for the JJA season, which implies that the southerly flow is strongly correlated with local evaporation. The negative SST anomalies over the eastern IO trigger the positive IOD event, which is

supported by previous studies (Li et al. 2002; Sooraj et al. 2009).

It is worthwhile to note that there is a clear asymmetry in the ENSO-IOD coupling process between the El Nino and La Nina. For example, the precipitation anomalies over the off-equatorial western Pacific much effectively affects to the variability over the eastern IO during the La Nina. We calculated the conditional correlation, and found that the correlation during MAM between the precipitation over the off-equatorial western Pacific and the meridional wind over the eastern IO is 0.35 during the El Nino (i.e. off-equatorial western Pacific >0), and 0.53 during the La Nina (i.e. off-equatorial western Pacific <0). This asymmetry is even stronger in JJA season (i.e. correlation during the El Nino is 0.12, that during the La Nina is 0.82). In addition, the asymmetry is also clear in the relationship between the meridional wind over the eastern IO and the evaporation, that the correlation between them during MAM season is 0.50 during the El Nino (i.e. meridional wind over the eastern IO >0), and 0.70 during the La Nina (i.e. meridional wind over the eastern IO <0).

In addition, meridional wind can induce precipitation changes via advection of moist energy. Ham et al. (2007) showed that equatorward flow over the maritime continent advects dry-cold moist energy from high latitudes, and then induces local downward motion during the El Nino peak season. Similarly, positive anomalous precipitation over the off-equatorial western Pacific can induce cross-equatorial southerly flow, which can cause advection of dry-cold moist energy, inducing an anomalous downward motion (i.e., negative precipitation) as the meridional gradient of climatological moist energy is positive south of 5° N. To support this argument, Fig. 6a shows a relationship between the anomalous precipitation over the off-equatorial western Pacific and the 850-hPa anomalous meridional flow over the maritime continent (120° E– 150° E, 10° S– 0°). The relationship between the 850-hPa meridional wind and the precipitation over the maritime continent is demonstrated to

Fig. 6 **a** Scatter diagram for precipitation anomalies over the off-equatorial western Pacific (120°–160°E, 0°–15°N) and 850-hPa meridional wind over the maritime continent (120°–150°E, 10°–0°S); **b** scatter diagram for 850-hPa meridional wind and precipitation anomalies over the maritime continent (120°–150°E, 10°–0°S)



some extent by correlation coefficient of 0.44 for the MAM season and 0.38 for the JJA season, which are significant at 95 % confidence level. This denotes that the positive anomalous precipitation over the off-equatorial western Pacific might possibly induce the southerly flow over the maritime continent. To examine whether the southerly flow over the maritime continent is associated with the local negative precipitation anomalies, Fig. 6b shows a scatter diagram between the 850-hPa anomalous meridional wind and the anomalous precipitation over the maritime continent. A clear negative relationship is indicated by correlation coefficients of -0.41 for the MAM season and -0.61 for the JJA season, denoting that the southerly flow over the maritime continent can induce negative precipitation anomalies over the same area. It is worthwhile to note that the precipitation over the off-equatorial western Pacific affects 850 hPa meridional wind over the maritime continent much effectively during the La Nina, while the southerly is coupled to the negative precipitation strongly during the El Nino (not shown).

In short, there are two possible explanations for how the ENSO-related positive anomalous precipitation over the off-equatorial western Pacific can induce the IOD. The first is that the positive anomalous precipitation over the off-equatorial western Pacific induces southerly flow over the eastern IO, which increases evaporation by enhancing total wind speed. Then, the negative SST anomalies over the eastern IO generate locally suppressed motions, which can induce the equatorial easterly anomalies over the IO basin, to excite a positive IOD event. The other explanation is low-level moist advection due to southerly flow. Over the southern hemisphere, where the meridional moist energy gradient is positive, this southerly flow can induce dry-cold moist energy advection, inducing the suppressed motions.

To investigate whether there is a significant difference in the physical processes linking ENSO and IOD, Fig. 7 shows the 850-hPa meridional flow over the eastern IO and

maritime continent (90°E–150°E, 10°S–0°) and the evaporation over the eastern IO (90°E–110°E, 10°S–0°) for the MAM and JJA seasons regressed onto the DJF Nino3.4 index during 1979–1998 and 1999–2014. In addition, the vertically averaged (1000–500 hPa) moist energy advection due to the wind anomalies ($-v' \frac{\partial \bar{m}}{\partial y}$, where \bar{m} is the climatological moist energy, and v' is the anomalous meridional wind) over the maritime continent (120°E–150°E, 10°S–0°) is also shown. Note that the advection of climatological moist energy due to the anomalous wind vector is the largest term among all linearized moist energy advection terms (not shown). The error-bar in the recent decade denotes 95 % confidence level using the bootstrap method (Yeh et al. 2009). That is, we randomly select the 16 years within whole period (i.e. 1979–2014), and calculate the regression coefficients with the selected years. This process is repeated 10,000 times to obtain the probability distribution function (PDF) of the regression coefficient. Finally, the upper 2.5 % and lower 2.5 % value is obtained to draw the error range.

The ENSO-related cross-equatorial meridional flow over the eastern IO and the maritime continent during the MAM seasons of 1999–2014 is three times smaller than that for 1979–1998. The same cross-equatorial southerly flow during the JJA seasons of 1979–1998 is still stronger, though the difference is reduced. Consistent with the weaker cross-equatorial southerly flow over the maritime continent in recent decades, the amplitude of evaporation is systematically reduced (Fig. 7b), along with a weakened negative moist energy advection (Fig. 7c) for the both the MAM and JJA seasons of 1999–2014. This reduced evaporation is linked to weaker negative anomalous SST for a positive IOD over the eastern IO. In addition, weaker moisture advection signals can weaken the amplitude of the negative precipitation anomaly over the maritime continent and the equatorial easterly over the IO, which also weakens the IOD variability during the ENSO in the 2000s and 2010s.

Fig. 7 **a** Area-averaged (90°–150°E, 10°–0°S) 850-hPa meridional wind anomalies (ms^{-1}) over the eastern IO and western Pacific, **b** latent heat flux anomalies (Wm^{-2}) over the eastern IO (90°–110°E, 10°–0°S), **c** moist energy advection due to anomalous meridional wind ($\text{J kg}^{-1} \text{s}^{-1}$) over 1000–500 hPa over the maritime continent (120°–150°E, 10°–0°S), regressed onto the DJF Nino3.4 index. The *error-bar* in the recent decade denotes the 95 % confidence level based on the bootstrap method

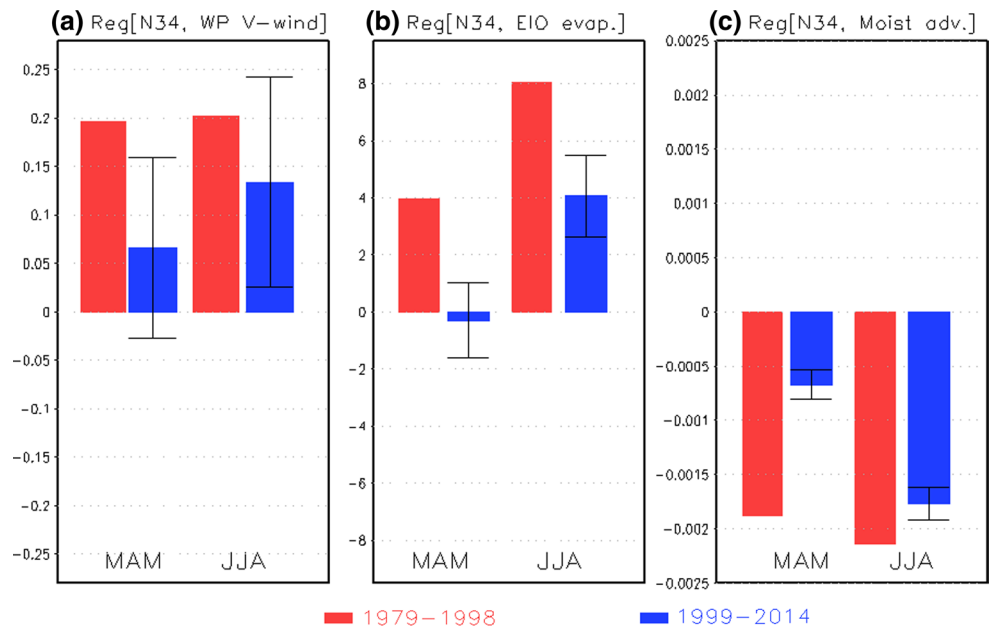
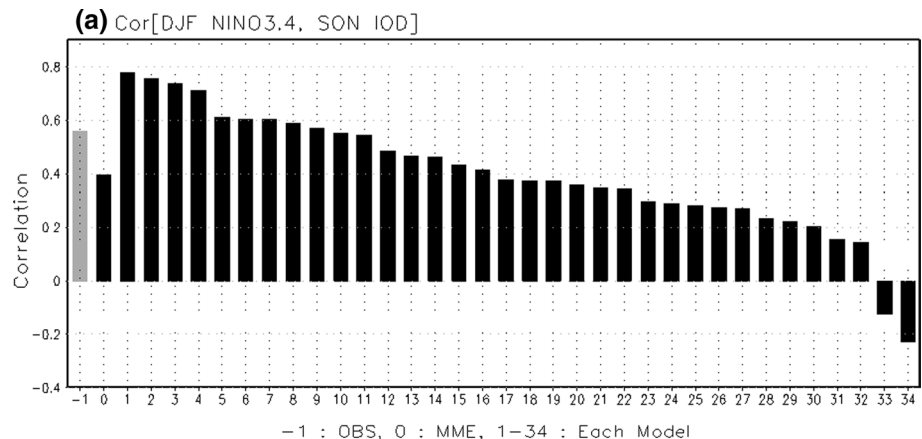


Fig. 8 Correlation between the IOD during the SON season and the Nino3.4 index during the DJF season for each of the CMIP5 models



4 CMIP5 analysis

To investigate what controls the ENSO–IOD coupling, 34 CMIP5 models were analyzed. To quantify the strength of ENSO–IOD coupling in each model, the correlation between the SON IOD and the DJF Nino3.4 index was calculated for each model and is shown in Fig. 8. This correlation roughly represents the strength of the ENSO–IOD coupling. The observed ENSO–IOD coupling strength is 0.55 for the period of 1979–2014, and the multi-model ensemble (MME) value is slightly lower than 0.4, which means the observed ENSO–IOD relationship is simulated to some extent in the CMIP5 models. With the exception of two models, most of the models exhibit positive ENSO–IOD coupling strength. It is interesting that the correlation in the CMIP5 models varies from about 0.8 to –0.2, implying that the degree of ENSO–IOD coupling is quite

different from model to model. To examine what controls ENSO–IOD coupling, we categorized the models into two groups: models number 1–10 belong to the “strong ENSO–IOD Coupling (strong EIC)” models, while models number 25–34 belong to the “weak ENSO-IOD Coupling (weak EIC) models.” Note that the “strong EIC models” generally simulate a degree of ENSO–IOD coupling strength similar to the observed strength. Therefore, it is interesting to compare the inter-decadal variation of the ENSO–IOD coupling strength in the “strong EIC models” with the observed features discussed in the previous chapter.

Before analyzing inter-decadal variation of the ENSO–IOD coupling strength in the “strong EIC models,” it is worthwhile to check whether the models simulate realistic ENSO and IOD amplitudes, as the timing of ENSO and IOD development might be important for simulating realistic ENSO–IOD coupling mechanisms. Figure 9 shows the

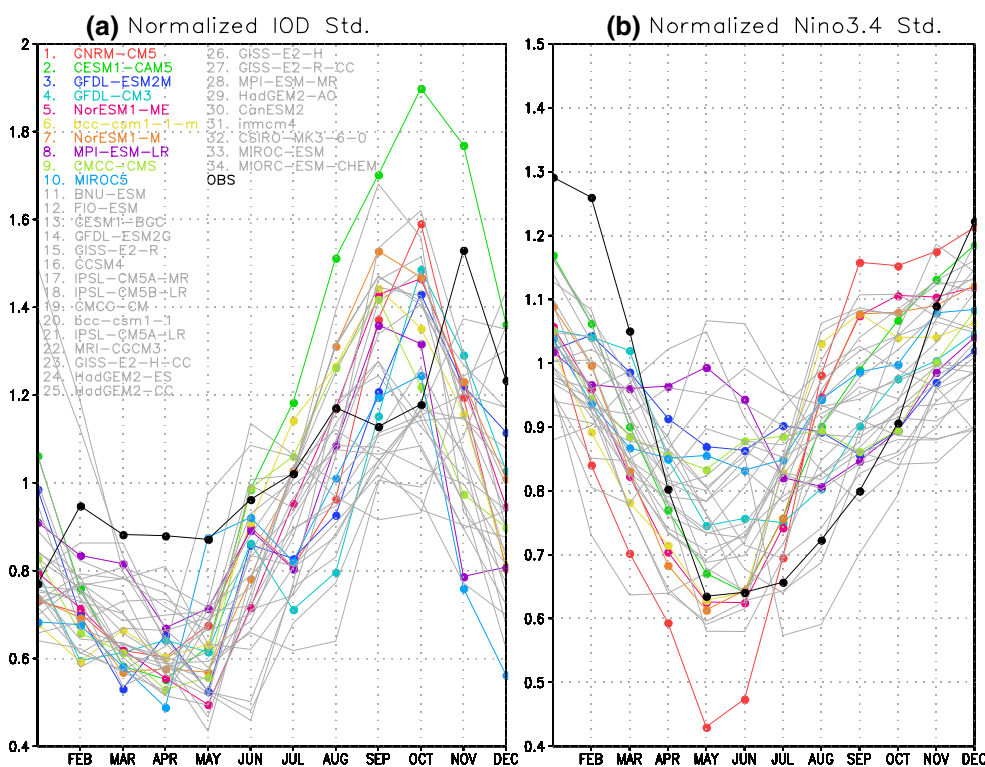


Fig. 9 Monthly standard deviation of the **a** IOD index and **b** Nino3.4 index for 34 CMIP5 models and observation (*black*). The monthly standard deviation is normalized by standard deviation using all seasons. “Strong EIC models” are denoted by *colored lines*

monthly standard deviation (std) of the IOD and Nino3.4 indices in all CMIP5 models, with the “strong EIC models” denoted by colored lines. The observed IOD std exhibits a peak phase during the boreal fall season especially during November, and of the CMIP5 models simulate the observed peak in the IOD index to some extent (Jourdain et al. 2013). In addition, the observed boreal winter peak of the Nino3.4 index is well simulated in most of the “strong EIC models.” It is clear that most of the “strong EIC models” simulate the observed seasonal IOD and ENSO peaks.

To investigate the inter-decadal variation of the ENSO–IOD coupling in the “strong EIC models,” the 15-year moving correlation between the SON IOD index and the DJF Nino3.4 index was calculated (not shown). Then, decades with strong (weak) ENSO–IOD coupling were defined as the decades when the difference between the 15-year moving correlation and the time-averaged value was greater (less) than 1 (–1) std. Finally, the Nino3.4-regressed precipitation, SST, and the 850-hPa meridional wind were calculated for strong and weak ENSO–IOD coupling decades. Figure 10 shows the Nino3.4-regressed precipitation, SST and 850-hPa meridional wind anomalies of the “strong EIC models” for strong and weak ENSO–IOD coupling decades during the El Niño developing AMJ season. For both cases, the positive precipitation anomalies over the western Pacific is shown along with the negative anomalous

precipitation over the maritime continent. In addition, the positive SST anomalies over the equatorial central-eastern Pacific are clear, denoting the El Niño signal. It is interesting that the positive SST anomalies over the central Pacific is extended to the north, which is dynamically consistent with the local positive precipitation anomalies. The southerly flow over the maritime continent, induced by the positive anomalous precipitation in the western Pacific, is also shown for both decades. However, ENSO-related positive anomalous precipitation over the western Pacific is systematically stronger during strong ENSO–IOD coupling decades. This is also reflected in the difference map of the strong and the weak ENSO–IOD coupling decades. Consistently, the southerly flow over the maritime continent is systematically stronger during strong ENSO–IOD coupling decades. This implies that the off-equatorial positive precipitation anomalies during the ENSO developing phase are crucial for a strong ENSO–IOD coupling in climate models, which is consistent with the observational findings.

In addition to the inter-decadal variation in individual models, it might be worthwhile to examine whether the large inter-model diversity on the ENSO–IOD coupling strength shown in Fig. 8 is caused by similar factors. As shown in Fig. 9, most of the climate models, including the “weak EIC models,” simulate a realistic ENSO and IOD seasonal phase-locking, which implies that there would

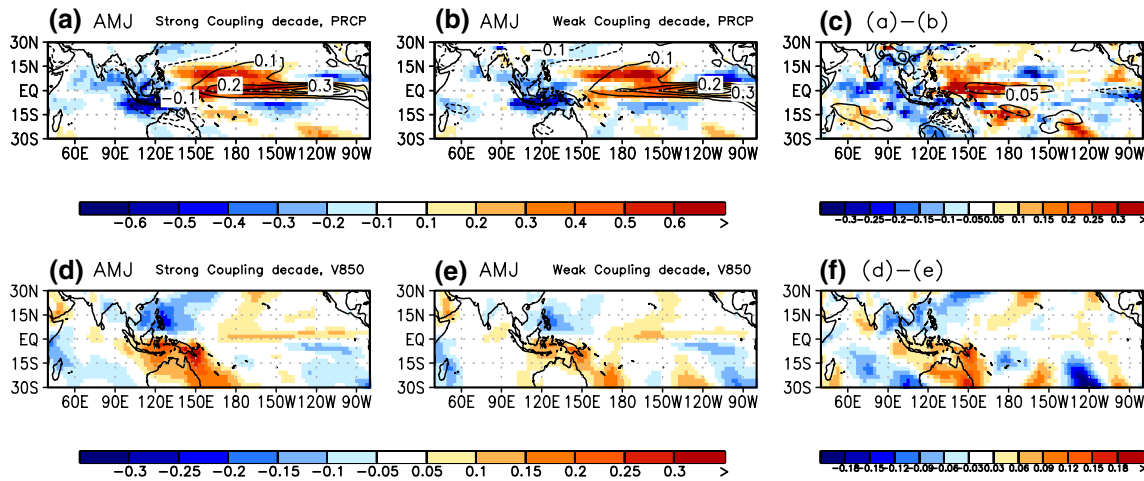


Fig. 10 Nino3.4-regressed precipitation (*shading in upper panels*), SST (*contour in upper panels*), and 850-hPa meridional wind anomalies (*lower panels*) for the AMJ seasons during strong ENSO-IOD coupling decades (*right*) and weak ENSO-IOD coupling decades

(*middle*) in the “strong EIC models.” The differences of Nino3.4-regressed **c** precipitation and **f** 850-hPa meridional wind between two groups are also shown

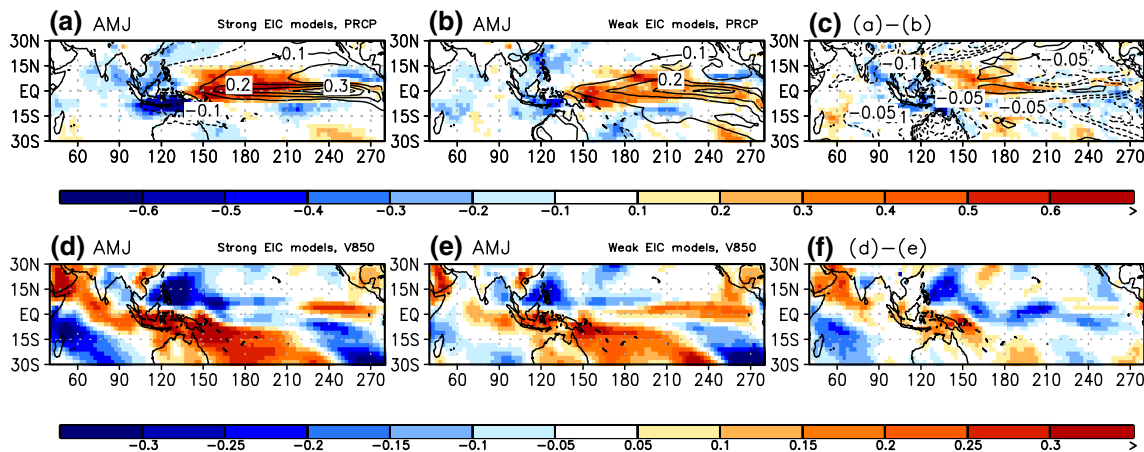


Fig. 11 Nino3.4-regressed precipitation (*shading in upper panels*), SST (*contour in upper panels*), and 850-hPa meridional wind anomalies (*lower panels*) during the AMJ season in “strong EIC models”

(*right*) and “weak EIC models” (*middle*). The differences of Nino3.4-regressed **c** precipitation and **f** 850-hPa meridional wind between two groups are also shown

be a dynamical reason that determines the ENSO-IOD coupling strength in climate models. To investigate what causes the different ENSO-IOD coupling strengths among climate models, Fig. 11 shows the AMJ ENSO-related precipitation and 850-hPa meridional wind by calculating the regression with respect to the DJF Nino3.4 index in the “strong EIC models” and the “weak EIC models.” The “strong EIC models” tend to simulate stronger positive precipitation over the off-equatorial western Pacific compared to models with the lowest ENSO-IOD coupling strength along with the slightly stronger local positive SST anomalies (Fig. 11a, b). In addition, the negative precipitation

anomaly over the maritime continent is also stronger in the “strong EIC models,” which is dynamically consistent with the cross-equatorial southerly flow over the maritime continent as a Gill-type response (Gill 1980). It is clearly shown that the “strong EIC models” tend to simulate a stronger cross-equatorial southerly flow over the maritime continent, which is quite consistent with the observed inter-decadal change in the ENSO-IOD relationship. Therefore, the inter-model differences in ENSO-IOD coupling strength of the CMIP5 models support the observational arguments regarding the inter-decadal change in the ENSO-IOD relationship between 1979–1998 and 1999–2014.

5 Summary and discussion

This study reports a recent weakening of the ENSO–IOD coupling for 1999–2014 compared to the two previous decades (1979–1998). The 15-year moving correlation between the ENSO and the IOD is systematically smaller during the 2000s and 2010s compared to the two preceding decades. During the developing phase of the El Niño, the positive anomalous precipitation over the northern off-equatorial western Pacific becomes systematically weaker during 1999–2014. This weakens the low-level cross-equatorial southerly anomalies over the maritime continent, which also weakens the local negative precipitation anomaly through cold and dry moist energy advection. As this negative precipitation anomaly over the maritime continent acts to induce the equatorial easterly over the IO, which activates the positive IOD event via air–sea interaction, the weak negative precipitation over the maritime continent suppresses the ENSO-related IOD variability. In addition, weak cross-equatorial southerly flow leads to less evaporation with a weaker negative anomalous SST over the eastern IO. In the CMIP5 models with realistic ENSO–IOD coupling strength (i.e., the “strong EIC models”), the ENSO-related cross-equatorial southerly flow and the associated suppressed convection over the maritime continent during the strong ENSO–IOD coupling decade are significantly stronger than that during the weak ENSO–IOD coupling decade, supporting observational data. In addition, there is a huge inter-model diversity in the ENSO–IOD coupling strength, and it is found that the ENSO-related off-equatorial positive anomalous precipitation over the western Pacific and the related southerly flow are systematically enhanced in models whose ENSO–IOD coupling strength is stronger than that of other models.

One can wonder whether the recent La Niña-like background state change, which is closely linked to the hiatus warming in 2000s (Kosaka and Xie 2013; Meehl et al. 2014), is responsible for the recent weakening ENSO–IOD coupling strength. McGregor et al. (2014) and Hong et al. (2013) argued the role of Atlantic SST warming on this La Niña-like cooling, and Luo et al. (2012) emphasized the Indian Ocean warming. The stronger Indian Ocean warming due to the global warming would extend the warm-pool area with increased climatological convection over the Indian Ocean, and which might lead to a higher chance that the IOD is induced through intrinsic air–sea coupled feedback within the Indian Ocean. Also, it is possible that the cold background condition over the eastern Pacific would weaken the local convection anomalies during the El Niño (Kim et al. 2011; Watanabe et al. 2012; Ham and Kug

2012), therefore, overall atmospheric El Niño teleconnection would be also weakened. This implies that the recent La Niña-like background change might play some roles in the weakening of the ENSO–IOD coupling strength during 1999–2014.

This inter-decadal modulation in the ENSO–IOD relationship is a key to understand the teleconnection pattern during the ENSO, especially over regions close to the Indian Ocean. For example, the weakening of the ENSO–IOD coupling during the 2000s could have reinforced the ENSO–ISMR relationship, which had been weakened during previous decades (Kumar et al. 1999; Ashok et al. 2001). To check whether this argument can be applied to the recent inter-decadal change of the ENSO–IOD coupling, we calculated the correlation between the area-averaged precipitation over the IO (60°E–95°E, 5°N–35°N) during the JJA season and the DJF Niño3.4 index for 1979–1998 and 1999–2014. The correlation between JJA rainfall and ENSO for 1999–2014 is -0.55 , while for 1979–1998 it is nearly zero (-0.04). This shows that the coupling between the ENSO and IO rainfall becomes significant in the 2000s and 2010s, together with a weakening of the ENSO–IOD coupling. Kumar et al. (2006) discovered that El Niño with strong ENSO–ISMR coupling have a stronger SST signal over the Central Pacific (CP) than other El Niño. Based on their argument, it is possible that the strong coupling between ENSO and the ISMR in the 2000s might be due to the coupling between the CP El Niño and the ISMR as the generation of the CP El Niño systematically increased in the 2000s (Yeh et al. 2009, 2014).

In addition, even though Kumar et al. (2006) did not mention explicitly, the impact of the CP-type El Niño on the IOD can be inferred in their paper. In their Fig. 2, the additional warming over the central Pacific can lead a dipole pattern of the precipitation anomalies over the Indian Ocean. The precipitation is reduced over the western IO, while that is increased over the eastern IO, which is dynamically linked to the equatorial westerly, therefore the negative IOD. This implies that the stronger warming over the central Pacific during the CP El Niño, which is frequently induced in the 2000s, can weaken the typical impact of the positive ENSO–IOD relationship. This feature is reflected to some extent in the Niño3.4-related SST fields (Fig. 3a, b), which show that the positive SST peak over the equatorial Pacific was slightly extended to the west in the 2000s, when the ENSO–IOD relationship was weakened. Based on these findings, it is worthwhile to dig up the role of the CP El Niño in Indian Ocean variability separately from that of the canonical El Niño to enhance society’s understanding of recent changes in the ENSO–IOD, and ENSO–ISMR relationships.

Acknowledgments This work was supported by the National Research Foundation of Korea (NRF) grant funded by the Korea government (MSIP) (NRF-2015R1C1A1A02036846). JSKI is supported by the Korea Meteorological Administration Research and Development Program under grant KMIPA 2015-1041.

References

- Adler RF et al (2003) The version-2 global precipitation climatology project (GPCP) monthly precipitation analysis (1979-present). *J. Hydrometeorol* 4(6):1147–1167
- Allan RJ et al (2001). Is there an Indian Ocean dipole and is it independent of the El Niño-Southern Oscillation?. International CLIVAR Project Office
- Ashok K, Saji NH (2007) On the impacts of ENSO and Indian Ocean dipole events on sub-regional Indian summer monsoon rainfall. *Nat Hazards* 42(2):273–285. doi:10.1007/s11069-006-9091-0
- Ashok K et al (2001) Impact of the Indian Ocean dipole on the relationship between the Indian monsoon rainfall and ENSO. *Geophys Res Lett* 28(23):4499–4502
- Ashok K, Guan ZY, Saji NH, Yamagata T (2004) Individual and combined influences of ENSO and the Indian Ocean Dipole on the Indian summer monsoon. *J Clim* 17:3141–3155
- Baquero-Bernal A et al (2002) On dipolelike variability of sea surface temperature in the tropical Indian Ocean. *J Clim* 15(11):1358–1368
- Behera SK, Yamagata T (2003) Influence of the Indian Ocean dipole on the Southern Oscillation. *J Meteorol Soc Jpn* 81(1):169–177
- Behera S et al (2000) Simulation of interannual SST variability in the tropical Indian Ocean. *J. Clim* 13(19):3487–3499
- Behera SK, Luo J-J, Masson S, Rao SA, Sakuma H, Yamagata T (2006) A CGCM study on the interaction between IOD and ENSO. *J Clim* 19:1688–1705
- Cai W et al (2011) Interactions of ENSO, the IOD, and the SAM in CMIP3 models. *J Clim* 24(6):1688–1704
- Dee DP, Uppala SM, Simmons AJ, Berrisford P, Poli P, Kobayashi S, Vitart F (2011) The ERA-Interim reanalysis: configuration and performance of the data assimilation system. *Q J R Meteorol Soc* 137(656):553–597
- Gill AE (1980) Some simple solutions for heat-induced tropical circulation. *R Meteorol Soc Q J* 106:447–462
- Ham Y-G, Kug J-S (2012) How well do current climate models simulate two types of El Niño? *Clim Dyn* 39:383–398. doi:10.1007/s00382-011-1157-3
- Ham YG, Kug J-S (2015) Improvement of ENSO simulation based on intermodel diversity. *J Clim* 28:998–1015
- Ham Y-G, Kug J-S, Kang I-S (2007) Role of moist energy advection in formulating anomalous Walker Circulation associated with El Niño. *J Geophys Res* 112, D24105. doi:10.1029/2007JD008744
- Hong CC, Lu MM, Kanamitsu M (2008) Temporal and spatial characteristics of positive and negative Indian Ocean dipole with and without ENSO. *J Geophys Res Atmos* 113:D08107
- Hong CC, Li T, Chen YC (2010) Asymmetry of the Indian Ocean basinwide SST anomalies: roles of ENSO and IOD. *J Clim* 23(13):3563–3576
- Hong S, Kang IS, Choi I, Ham YG (2013) Climate responses in the tropical Pacific associated with Atlantic warming in recent decades. *Asia Pac J Atmos Sci* 49(2):209–217
- Iizuka S et al (2000) The Indian Ocean SST dipole simulated in a coupled general circulation model. *Geophys Res Lett* 27(20):3369–3372
- Izumo T, Vialard J, Lengaigne M, de Boyer Monte'gut C, Behera SK, Luo JJ, Cravatte S, Masson S, Yamagata T (2010) Influence of the Indian Ocean Dipole on following year's El Niño. *Nat Geosci* 3:168–172
- Izumo T, Lengaigne M, Vialard J, Luo JJ, Yamagata T, Madec G (2014) Influence of Indian Ocean Dipole and Pacific recharge on following year's El Niño: interdecadal robustness. *Clim Dyn* 42(1–2):291–310
- Jin FF (1997) An equatorial ocean recharge paradigm for ENSO. Part I: Conceptual model. *J Atmos Sci* 54(7):811–829
- Jourdain NC, Gupta AS, Taschetto AS, Ummenhofer CC, Moise AF, Ashok K (2013) The Indo-Australian monsoon and its relationship to ENSO and IOD in reanalysis data and the CMIP3/CMIP5 simulations. *Clim Dyn* 41(11–12):3073–3102
- Kim D, Jang Y-S, Kim D-H, Kim Y-H, Watanabe M, Jin F-F, Kug J-S (2011) El Niño-Southern Oscillation sensitivity to cumulus entrainment in a coupled general circulation model. *J Geophys Res* 116:D22112. doi:10.1029/2011JD016526
- Kosaka Y, Xie SP (2013) Recent global-warming hiatus tied to equatorial Pacific surface cooling. *Nature* 501(7467):403–407
- Kug J-S, Ham Y-G (2012) Indian Ocean feedback to the ENSO transition in a multi-model ensemble. *J Clim* 25:6942–6957. doi:10.1175/JCLI-D-12-00078.1
- Kug J-S, Kang I-S (2006) Interactive feedback between the Indian Ocean and ENSO. *J Clim* 19:1784–1801
- Kug J-S, Li T, An S-I, Kang I-S, Luo J-J, Masson S, Yamagata T (2006a) Role of the ENSO-Indian Ocean coupling on ENSO variability in a coupled GCM. *Geophys Res Lett* 33:L09710. doi:10.1029/2005GL024916
- Kug J-S, Kirtman BP, Kang IS (2006b) Interactive Feedback between ENSO and the Indian Ocean in an interactive coupled model. *J Clim* 19(24):6371–6381
- Kug J-S, Sooraj KP, Li T, Jin F-F (2010) Precursors of El Niño/La Niña onset and their interrelationship. *J Geophys Res* 115:D05106. doi:10.1029/2009JD012861
- Kumar KK et al (1999) On the weakening relationship between the Indian monsoon and ENSO. *Science* 284(5423):2156–2159
- Kumar KK et al (2006) Unraveling the mystery of Indian monsoon failure during El Niño. *Science* 314(5796):115–119
- Lau N-C, Nath MJ (2004) Coupled GCM simulation of atmosphere-ocean variability associated with zonally asymmetric SST changes in the tropical Indian Ocean. *J Clim* 17:245–265
- Li T, Zhang Y, Lu E, Wang D (2002) Relative role of dynamic and thermodynamic processes in the development of the Indian Ocean dipole: an OGCM diagnosis. *Geophys Res Lett* 29:2110. doi:10.1029/2002GL015789
- Li T, Wang B, Chang CP, Zhang Y (2003) A theory for the Indian ocean dipole-zonal mode*. *J Atmos Sci* 60(17):2119–2135
- Luo J-J, Zhang R, Behera S, Masumoto Y, Jin F-F, Lukas R, Yamagata T (2010) Interaction between El Niño and extreme Indian Ocean dipole. *J Clim* 23:726–742
- Luo JJ, Sasaki W, Masumoto Y (2012) Indian Ocean warming modulates Pacific climate change. *Proc Natl Acad Sci* 109(46):18701–18706
- McGregor S, Timmermann A, Stuecker MF, England MH, Merrifield M, Jin FF, Chikamoto Y (2014) Recent Walker circulation strengthening and Pacific cooling amplified by Atlantic warming. *Nat Clim Change* 4(10):888–892
- Meehl GA, Teng H, Arblaster JM (2014) Climate model simulations of the observed early-2000s hiatus of global warming. *Nat Clim Change* 4(10):898–902
- Rayner NA, Parkler DE, Horton EB, Folland CK, Alexander LV, Rowell DP, Kent EC, Kaplan A (2003) Global analyses of sea surface temperature, sea ice, and night marine air temperatures since the late nineteenth century. *J Geophys Res*. doi:10.1029/2002JD002670
- Reynolds RW, Rayner NA, Smith TM, Stokes DC, Wang W (2002) An improved in situ and satellite SST analysis for climate. *J. Clim* 15:1609–1625

- Saji N et al (1999) A dipole mode in the tropical Indian Ocean. *Nature* 401(6751):360–363
- Sooraj K et al (2009) Impact of El Niño onset timing on the Indian Ocean: pacific coupling and subsequent El Niño evolution. *Theor appl climatol* 97(1–2):17–27
- Smith TM, Reynolds RW (2004) Improved extended reconstruction of SST (1854–1997). *J Clim* 17(12):2466–2477
- Ueda H, Matsumoto J (2000) A possible process of east-west asymmetric anomalies over the Indian Ocean in relation to 1997/98 El Niño. *J Meteor Soc Japan* 78:803–818
- Ummenhofer CC et al (2011) Multi-decadal modulation of the El Niño-Indian monsoon relationship by Indian Ocean variability. *Environ Res Lett* 6(3):034006
- Watanabe M, Kug J-S, Jin F-F, Collins M, Ohba M, Wittenburg A (2012) Uncertainty in the ENSO amplitude change from the past to the future. *Geophys Res Lett* 39:L20703. doi:[10.1029/2012GL053305](https://doi.org/10.1029/2012GL053305)
- Webster PJ et al (1999) Coupled ocean–atmosphere dynamics in the Indian Ocean during 1997–98. *Nature* 401(6751):356–360
- Weller E, Cai W (2013) Asymmetry in the IOD and ENSO teleconnection in a CMIP5 model ensemble and its relevance to regional rainfall. *J Clim* 26(14):5139–5149
- Yeh S-W et al (2009) El Niño in a changing climate. *Nature* 461(7263):511–514
- Yeh S-W, Kug J-S, An S-I (2014) Recent progress on two types of El Niño: observations, dynamics, and future changes. *Asia Pac J* 50:69–81. doi:[10.1007/s13143-014-0028-3](https://doi.org/10.1007/s13143-014-0028-3)
- Yuan Y, Li C (2008) Decadal variability of the IOD-ENSO relationship. *Chinese Sci Bulletin* 53(11):1745–1752